ABSTRACT

Title of dissertation: Direct measurement of a Feshbach resonance with imaging

and measuring topology of BECs in a synthetic dimensions

Dina Genkina
Doctor of Philosophy, 2018

Dissertation directed by: Professor Ian Spielman
Department of Physics

Direct measurement of a Feshbach resonance with imaging of s-wave scattering
and measuring topology of BECs in a synthetic dimensions lattice

by

Dina Genkina

Dissertation submitted to the Faculty of the Graduate School of the
University of Maryland, College Park in partial fulfillment
of the requirements for the degree of
Doctor of Philosophy
2018

Advisory Committee:
Professor Ian Spielman, Chair/Advisor

Chapter 4:   Synthetic dimensional lattice

In this chapter we explain the idea of an effective 2-D lattice with one real dimension created by lattice cites of a 1-D optical lattice and one 'synthetic' dimension created by treating the internal spin states of the atom as sites along a transverse axis. We do this by treating each dimension individually first. In the section 4.1, we describe 1-D optical lattices. We exlain the far off resonant interaction that leads to the AC Stark shift, and use it to write down the 1-D optical lattice Hamiltonian. We describe the often used tight binding approximation of the lattice Hamiltonian. We describe how the lattice is calibrated in our lab, and introduce Bloch oscillations.

In section 4.2, we describe the hyperfine structure of Rubidium, used as sites in the 'synthetic' dimension. We then describe two methods for coupling them to introduce tunneling in the synthetic dimensions: rf and Raman transitions. We describe the calibration procedures, and show ground states of the system with each of the couplings applied. In the last section, we combine the two dimensions and write out the full synthetic dimensions Hamiltonian. We plot the band structure, and describe the emergence of the effective magnetic field. We show the calibration procedure, and show the ground states of the system, featuring both bulk and edge satates with narrowing due to the magnetic length. We then show skipping orbits created by loading a superposition of states on the edge of the system, analagous to edge magnetoplasmons. The experiments in this section were detailed in the publication [1].

4.1 One dimensional optical lattices

The first, 'real' dimension in the synthetic dimensional lattice is discretized
into sites by an optical lattice. Optical lattices are a staple of cold atomic physics,
and are commonly used to emulate the crystal structure present in metals and other
condensed matter systems. In this section, we describe the orgin of the periodic
potential, derive the Hamiltonian and show how the lattice depth is detected and
calibrated in the lab.

4.1.1 Far off-resonant atom-light interaction

As described in section **??**, on timescales where spontaneous emission can
be neglected, two-level atoms exposed to laser radiation undergo coherent Rabi
oscillations between the two levels. Starting with c_g and c_e as the time-dependent
coefficients multiplying the eigenstate wavefuntions of the ground and excited state
respectively, and assuming the atom starts in the ground state $c_g(t = 0) = 1$, we
make the traditional transformation to the rotating frame:

$$c'_g(t) = c_g(t) \tag{4.1}$$

$$c'_e(t) = c_e(t)e^{-i\delta t}, \tag{4.2}$$

where δ is the detuning of laser light from resonance. In this frame, we can write
the atom-light Hamiltonian in the $\begin{pmatrix} c'_g \\ c'_e \end{pmatrix}$ basis as:

$$H = \hbar \begin{pmatrix} -\delta/2 & \Omega/2 \\ \Omega/2 & \delta/2 \end{pmatrix}, \tag{4.3}$$

where Ω is the coupling strength, also known as the Rabi frequency. In the limit of no coupling, $\Omega = 0$, in the rotating frame the eigenenegies are $E_{\pm} = \pm\hbar\delta/2$. For non-zero coupling, finding the eigenvalues of H gives $E_{\pm} = \pm\hbar\sqrt{\delta^2 + \Omega^2}/2$. Therefore, the bare (without light) eigenenrgies are shifted in the presence of the light.

For a far detuned laser beam, one expects that no absorption of the light will actually take place, and the atom will remain entirely in the ground state. Indeed, solving the Shroedinger equation with the above Hamiltonian

$$i\hbar\frac{d}{dt}\begin{pmatrix} c'_g \\ c'_e \end{pmatrix} = H \begin{pmatrix} c'_g \\ c'_e \end{pmatrix} \tag{4.4}$$

we obtain the oscillating excited state population

$$c'_e(t) = -i\frac{\Omega}{\sqrt{\Omega^2 + \delta^2}}\sin\left(\frac{\sqrt{\Omega^2 + \delta^2}t}{2}\right), \tag{4.5}$$

where the amplitude of the oscillation approches zero in the limit $\Omega \ll \delta$. Thus, the only effect of the light in this regime is to shift the eigenenergies of the ground and excited states. Expanding the energies in the small parameter Ω/δ, we obtain the shifted energies $E_{\pm} = \pm\hbar\sqrt{\delta^2 + \Omega^2}/2 \approx \pm(\delta/2 + \Omega^2/4\delta)$. The shift from bare energy levels is thus

$$\Delta E_{\pm} = \pm\Omega^2/4\delta. \tag{4.6}$$

This laser intensity dependent energy shift is called the AC Stark shift, and is the basis of most laser created potentials for cold atoms.

For the ground state, and a red detuned laser beam (where the laser frequency is lower than the resonant frequency), this creates energy minima in locations of maximal laser intensity. For the lattice described in this chapter, as well as for the trapping of our atoms in the final stages of cooling, we use high power (up to 10 W)

lasers with wavelength $\lambda_L = 1064$ nm.

4.1.2   Lattice Hamiltonian

Our 1-D optical lattice is created by retro-reflecting the $\lambda_L = 1064$ nm laser, creating a standing wave of light. Via the AC Stark shift, this creates a periodic potential for the atoms of the form

$$V = V_0 \sin^2(k_L x), \tag{4.7}$$

where $k_L = 2\pi/\lambda_L$ is the wavenumber associated with the lattice recoil momentum. The time-independent Hamiltonian, for some eigenenergy E_n, will be given by

$$-\frac{\hbar^2}{2m}\frac{d^2}{dx^2}\Psi_n(x) + V_0 \sin^2(k_L x)\Psi_n(x) = E_n\Psi_n(x). \tag{4.8}$$

Since the potential is spatially periodic, we can invoke Bloch's theorem [2]:

$$\Psi_{n,q} = e^{iqx} u_{n,q}(x), \tag{4.9}$$

where q is the crystal momentum restricted to $\pm\hbar k_L$, and $u_{n,q}(x)$ is the spatially varying part of the wavefunction. Plugging this in to the Hamiltonian, we obtain

$$-\frac{\hbar^2}{2m}\left(-q^2 + 2iq\frac{d}{dx} + \frac{d^2}{dx^2}\right)u_{n,q}(x) + V_0 \sin^2(k_L x)u_{n,q}(x) = E_n u_{n,q}(x). \tag{4.10}$$

Expanding $u_{n,q}(x)$ in Fourier components commensurate with the lattice period of $2k_L$ as $u_{n,q}(x) = \sum_{j=-\inf}^{\inf} a_j e^{i2k_L j x}$, we obtain

$$\sum_j \left(\frac{\hbar^2}{2m}(q + 2k_L)^2 a_j + V_0 \sin^2(k_L x)a_j\right) e^{i2k_L j x} = E_n \sum_j a_j e^{i2k_L j x}. \tag{4.11}$$

Re-writing $\sin^2(k_L x) = (e^{-2ik_L x} + e^{2ik_L x} - 2)/4$, multiplying both sides by $e^{i2k_L j' x}$ and invoking $\sum c_j e^{ik(j-j')} = \delta_{jj'}$, where $\delta_{jj'}$ is the Kroniker delta and c_j are appropriately normalized coefficients, we get for any value of the index j

$$\frac{\hbar^2}{2m}(q + 2k_L j)^2 a_j - \frac{V_0}{4}(a_{j+1} + a_{j-1}) = E_n a_j. \tag{4.12}$$

This can be expressed in matrix form

$$H_L = \begin{pmatrix} \ddots & & & & & \\ & \frac{\hbar^2}{2m}(q + 4k_L)^2 & \frac{V_0}{4} & 0 & 0 & 0 \\ & \frac{V_0}{4} & \frac{\hbar^2}{2m}(q + 2k_L)^2 & \frac{V_0}{4} & 0 & 0 \\ & 0 & \frac{V_0}{4} & \frac{\hbar^2}{2m}q^2 & \frac{V_0}{4} & 0 \\ & 0 & 0 & \frac{V_0}{4} & \frac{\hbar^2}{2m}(q - 2k_L)^2 & \frac{V_0}{4} \\ & 0 & 0 & 0 & \frac{V_0}{4} & \frac{\hbar^2}{2m}(q - 4k_L)^2 \\ & & & & & & \ddots \end{pmatrix}, \tag{4.13}$$

in the basis of momentum orders $|k\rangle = e^{ikx}$ given by:

$$\begin{pmatrix} \vdots \\ |q + 4k_L\rangle \\ |q + 2k_L\rangle \\ |q\rangle \\ |q - 2k_L\rangle \\ |q - 4k_L\rangle \\ \vdots \end{pmatrix}. \tag{4.14}$$

This matrix can be diagonalized for every value of the crystal momentum q, withthe resulting band structure shown in Figure 1. It is convenient to define the lattice recoil energy $E_L = \hbar^2 k_L^2/2m$. Then, we can re-write the Hamiltonian with
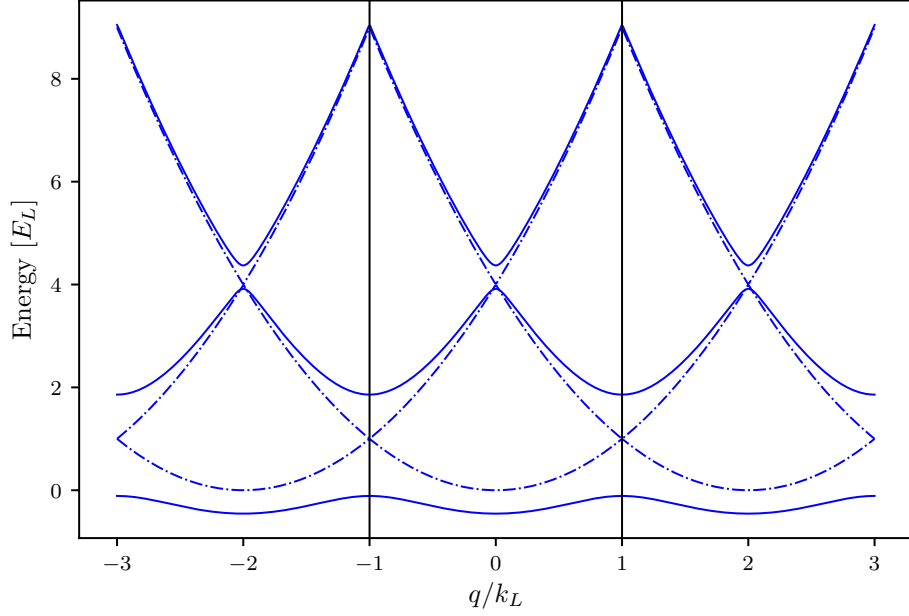
Figure 1: Lattice band structure in the extended zone scheme. The dashed lines represent the limit of zero lattice depth, with the regular parabolic dispersion relation of a free particle repating with reciprocal lattice period. The solid lines are the dispersion relation at $V_0 = 4.0E_L$, showing the opening of gaps at crossings of the zero lattice depth bands. The black lines demarcate the first Brillouin zone.

V_0 in units of E_L and momenta q in units of k_L as

$$
H_L/E_L =
\begin{pmatrix}
\ddots & & & & & \\
 & (q+4)^2 & \frac{V_0}{4} & 0 & 0 & 0 \\
 & \frac{V_0}{4} & (q+2)^2 & \frac{V_0}{4} & 0 & 0 \\
 & 0 & \frac{V_0}{4} & q^2 & \frac{V_0}{4} & 0 \\
 & 0 & 0 & \frac{V_0}{4} & (q-2)^2 & \frac{V_0}{4} \\
 & 0 & 0 & 0 & \frac{V_0}{4} & (q-4)^2 \\
 & & & & & \ddots
\end{pmatrix}.
\tag{4.15}
$$

In any numerical simulation, the number of momentum orders that can be included is finite. We determine the value of the parameter $n = \max(|j|)$ as the

lowest n at which the eigenvalues stop changing to machine precision from $n-1$. The code for finding and plotting the eigenvalues and eigenvectors of the lattice hamiltonian is included in Appendix [MAKE APPENDIX WITH CODE?].

4.1.3 Tight binding approximation

In the limit of large lattice depths, $V_0 >\approx 5E_L$, the lattice Hamiltonian is well approximated by the tight-binding model. In the tight binding model, the basis is assumed to be a set of orthogonal functions, called Wannier functions, localized to each lattice site $|j\rangle$. The approximation lies in assuming only nearest neighbor tunnelings between the sites, forming the tight-binding Hamiltonian

$$H_{\mathrm{tb}} = -t\,|j\rangle\,\langle j+1| + \text{H.c.}, \tag{4.16}$$

where t is the tunneling amplitude between nearest neighbor sites and H.c. stands for Hermitian conjugate. We have neglected the diagonal kinetic energy term, as it will be equal for every Wannier function $|j\rangle$ and thus represents a constant energy offset. All the information about the lattice depth is therefore reflected in the tunneling amplitude t.

The tight binding Hamiltonian can also be expressed in the momentum basis by Fourier transforming the basis functions:

$$|j\rangle = \frac{1}{\sqrt{N}} \sum_{k_j} e^{-ik_j j}\,|k_j\rangle\,, \tag{4.17}$$

giving the Hamiltonian

$$H_{\mathrm{tb}} = -\frac{1}{N} \sum_{k_1} \sum k_2 t e^{-ijk_1} e^{ik_2(j+1)}\,|k_1\rangle\,\langle k_2| + \text{H.c} = 2t\cos(k)\,|k\rangle\,\langle k|\,. \tag{4.18}$$

From this we can directly read off the band structure of the tight binding Hamilto-

nian. First, we notice that we only obtain one band - to approximate higher bands with the tight binding approximation we would need to construct a different set of Wannier functions and a different tunneling strength. Second, we see that the lowest band is simply a cosine - therefore we have solved for the band structure without even defining what the basis Wannier functions are! Third, the amplitude of the cosine function is given by the tunneling strength t. This gives us a good clue as to how to determine the appropriate tunneling given a lattice depth V_0 - simply find a t that matches the amplitude of the lowest band, which becomes cosinusoidal in the deep lattice limit.

The precise form of the Wannier functions depends on both the depth of the lattice and the band being reproduced. It is not necessary for us to find their full expression, as the band structure can be calculated without them. The definition, however, is

$$|j\rangle = \int_{\text{BZ}} e^{i\phi(q)-iqja}\Psi_q(x)\mathrm{d}q, \tag{4.19}$$

where the integral is over the Brillouin zone, from $-k_L$ to k_L, a is the lattice spacing $\lambda_L/2$, and Ψ_q is the Bloch wavefunction at crystal momentum q, and $\phi(q)$ is the phase associated with each Bloch wavefuntion. The Bloch wavefunctions individually have arbitrary phase. The phase plays an important role in combining the Bloch wavefunctions into a Wannier function, finding the proper phase relationship to make the wavefunction maximally localized at each site [3].

4.1.4   Pulsing vs adiabatic loading of the lattice

The lattice depth parameter $V_0/4$, for a range of values, can be well calibrated experimentally by pulsing on the lattice. Here, the word pulsing indicates that the lattice is turned on fully non-adiabatically, if not instantaneously, such that the original bare momentum state is projected onto the lattice eigenbasis, as shown

in Figure 3a. If the atoms start out stationary in the trap, the bare state in the momentum basis is simply

$$|\Psi_0\rangle = \begin{pmatrix} \vdots \\ 0 \\ 0 \\ 1 \\ 0 \\ 0 \\ \vdots \end{pmatrix}, \tag{4.20}$$

as depicted in Figure 3b.

Since the lattice eigenbasis is distinct from the bare one, instiantaneously turning on the lattice will necessarily excite the atoms into a superposition of lattice eigenstates, each evolving with a different phase according to the eigenenergy while the lattice is on, as shown in Figure 3c. Then, when the lattice is snapped back off, the wavefunction is projected back into the bare basis, and the varying phase accumulation results in a beating of the different momentum orders, see Figure 3d. This can be calculated simply by using the time evolution operator

$$|\Psi(t)\rangle = e^{-iH_L t/\hbar} |\Psi_0\rangle. \tag{4.21}$$

By pulsing on the lattice for variable amounts of time t, we can obtain fractional populations in the different momentum states. Time-of-flight imaging captures the momentum distribution of the cloud, and the different entries of $\Psi(t)$ in the momentum basis will thus appear as different clouds on the absorption image [IN-CLUDE IMAGES FROM PULSING DATA]. The fractional population in these clouds corresponds to a measurement of $|a_j|^2$. Typically for our values of the lattice depth $V_0 < 10E_L$, it is sufficient to simply count three central momentum orders,
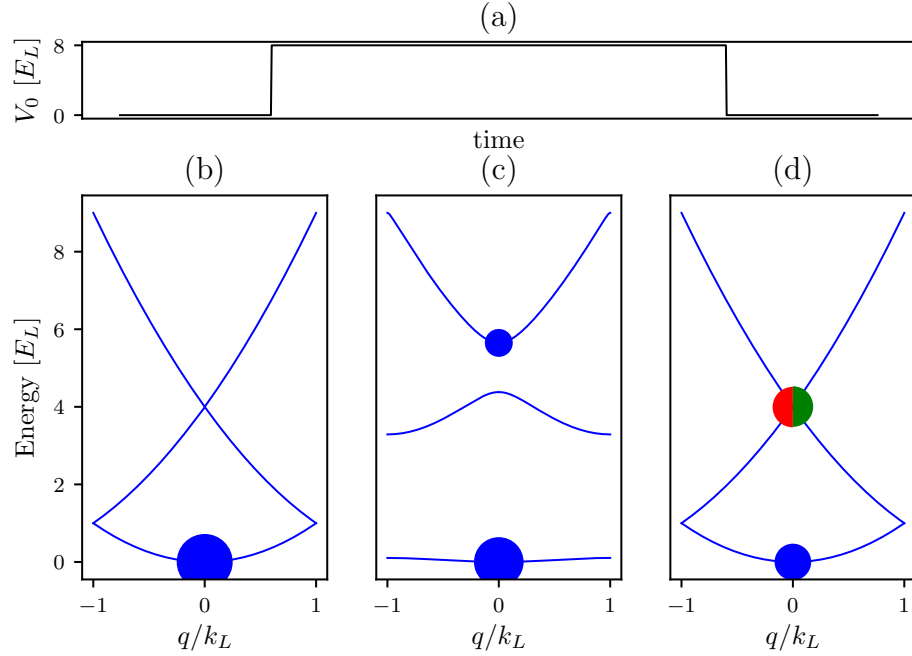
Figure 2: Lattice pulsing. (a) Lattice depth as a function of time during a pulsing experiment. The lattice is turned on instantaneously at $t = 0$ and held on for a variable amount of time until being turned off instantaneously at a final time $t = t_f$. (b) Atomic population before $t = 0$. The dispersion relation is that of a free particle, and all of the atoms start out at $q = 0$ in the lowest energy level. Here, the area of the dots is proportional to the fractional population in the energy state. (c) Atomic population after the lattice is turned on for a lattice depth of $V_0 = 8.0 E_L$. The energy spectrum now shows the lattice band structure, and some atomic population is projected onto the excited bands. (d) Atomic population after the lattice is snapped off at $t_f = 150$ μs. The wavefunction is projected back onto the bare states, with some fraction (blue circle) in the lowest band at $k = 0$ and some fraction in the excited band, with equal population being projected onto the $k = 2k_L$ (green) and $k = -2k_L$ (red).

$k = q, q \pm 2k_L$. Then, we can fit Eq. 4.21 to the data with fitting parameter V_0, thus deducing the lattuce depth. Some examples of these pulsing experiments are presented in figure [MAKE FIGURE]:

In contrast to pulsing, adiabatic loading turns the lattice on slowly, such that the atomic wavefunction starting in the bare ground state can continuously adjust to remain in the ground state of the current Hamiltonian, without projecting onto any of the higher bands. This process is illustrated in Figure 3. The adiabatic timescale depends on the spacing between the ground and next excited band (or if starting in a different eigenstate, the nearest eigenstate). If the energy difference between the ground and first excited state is ΔE, the timescale on which the lattice is turned on must fullfill $t \gg h/\Delta E$.

[FIND PICTURES OF ADIABATICALLY LOADED LATTICE STATES]

4.2   Raman and rf coupling

The second, 'synthetic' dimension in the effectively 2-D lattice is formed by the internal hyperfine states of the atoms, forming sites along a second dimension. To induce tunneling along the synthetic sites, analogous to lattice hopping between neighboring sites, we must engeneer some coupling between them. There are two ways we induce this tunneling - with rf coupling, tuned to be directly resonant with the energy difference between the hyperfine levels, and with two-photon Raman coupling, tuned such that the energy difference between the two photons matches the hyperfine splitting. In this section we describe the hypefine structure of ^{87}Rb, derive the Hamiltonians for both rf and Raman coupled states, and show how the Raman and rf coupled states are measured and calibrated in the lab.
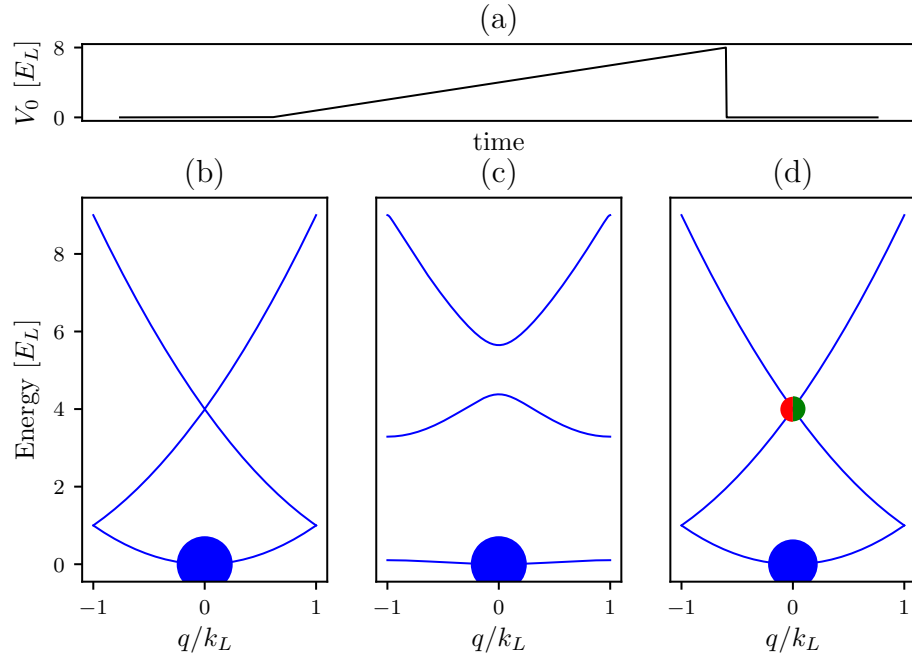
Figure 3: Adiabatic lattice loading. (a) Lattice depth as a function of time during adiabatic turn-on. The lattice is ramped on starting at $t = 0$, slowly increasng to a final lattice depth and turned off instantaneously at a final time $t = t_f$. (b) Atomic population before $t = 0$. All atoms are at $k = 0$ in the lowest bare band. (c) Atomic population after the lattice is turned on adiabatically to a lattice depth of $V_0 = 8.0 E_L$. All atoms remain in the lowest band, but the band is no longer bare. (d) Atomic population after the lattice is snapped off. The wavefunction is projected back onto the bare states, with some fraction (blue circle) in the lowest band at $k = 0$ and some fraction in the excited band, with equal population being projected onto the $k = 2k_L$ (green) and $k = -2k_L$ (red). Since the lowest lattice band is a superposition of bare bands, some atoms are excited to the higher bare bands.

4.2.1   Hyperfine structure

Alkali atoms' energy levels can be understood as primarily the energy state of the single electron in the outer shell. Fine structure arises from different combinations of angular momenta, including orbital angular momentum of the outermost electron with respect to the nucleus $\mathbf{L}$, the electron spin $\mathbf{S}$ and the nuclear spin $\mathbf{I}$. The total electron angular momentum is the combination of orbital and the spin angular momenta $\mathbf{J} = \mathbf{L} + \mathbf{S}$, and the quantum number can be any integer $|L - S| \leq J \leq |L + S|$. The ground state of ^{87}Rb, in term notation $^{2S+1}L_J$ is $^2S_{1/2}$, where S is orbital notation indicating $L = 0$. Since the total spin quantum number $J = 1/2$, this produces two possible spin projection quantum numbers, $m_J = \pm 1/2$.

There is also a contribution from the nuclear spin $\mathbf{I}$, resolvable at low magnetic fields, which gives rise to hyperfine structure of the states. For ^{87}Rb, $I = 3/2$. The total spin, including nuclear spin, is indicated by the quantum number F, and $|J - I| \leq F \leq |J + I|$. The interaction with the nuclear spin splits the ground state of ^{87}Rb into two manifolds, $F = 1$ and $F = 2$, with three hyperfine states in the $F = 1$ manifold ($m_F = 0, \pm 1$) and five hyperfine states in the $F = 2$ manifold ($m_F = 0, \pm 1, \pm 2$). These states couple to an external magnetic field B_z along some direction $\mathbf{e}_z$ via the Hamiltonian $H_B = \mu_B (g_J J_z + g_I I_z) B_z / \hbar$. Here μ_B is the Bohr magneton, and g_J and g_I are Lande g-factors. Since $g_J \gg g_I$, at high fields the nuclear spin interaction becomes small compared to the total energy shift, and the levels are grouped according to their m_J quantum number, as seen in Figure 4.

At low fields, however, the states are approximately linearly dependent on the m_F quantum number. The linear shift from the $B = 0$ states is known as the linear Zeeman shift. In the intermediate regime, the correction to the linear shift can be expressed in terms of and energy correction to each hyperfine state $\epsilon(B)|m_F|^2$, known as the quadratic Zeeman shift. For the magnetic fields used in experiments
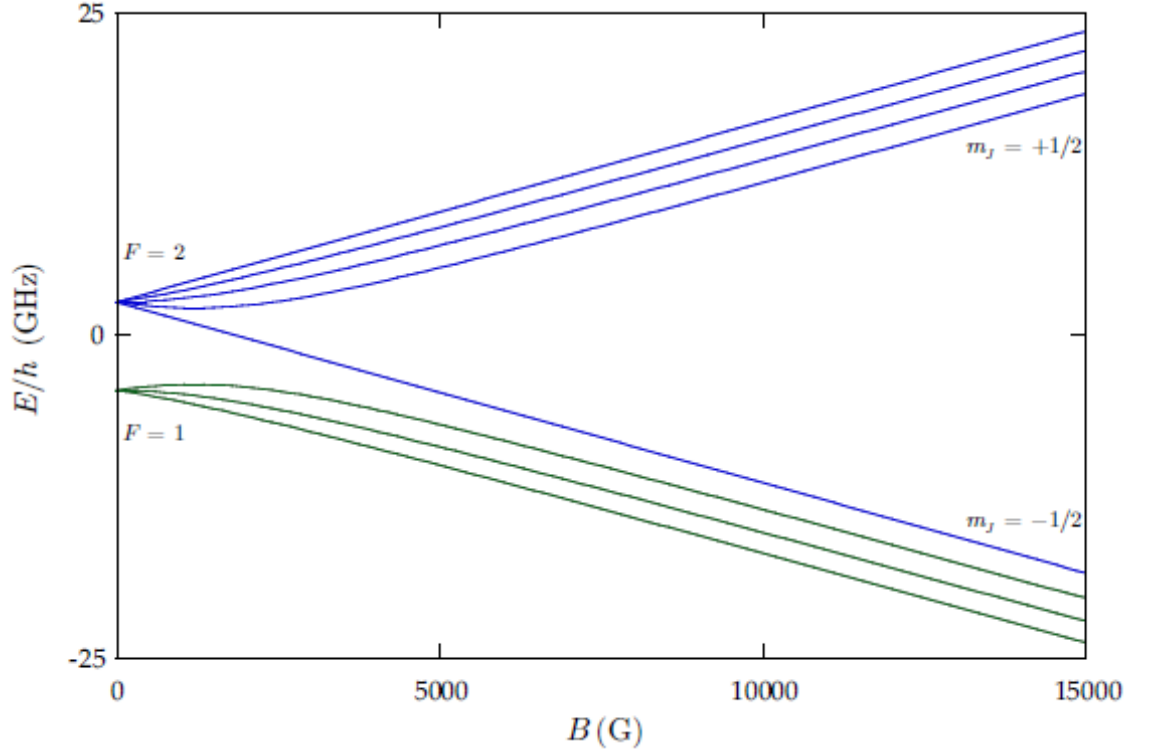
Figure 4: Energy structure of hyperfine states of the ground state of ^{87}Rb as a function of external magnetic field strength in Gauss. Figure from ref. [4]

described in this thesis, this correction is sufficient for describing the energy levels.

4.2.2   Raman and rf coupling Hamiltonians

For the $F = 1$ manifold, there are three available spin states $m_F = 0, \pm 1$. There are many ways of introducing coupling terms between the different hyperfine states. Here, we will explain two methods: rf coupling and Raman coupling. Rf coupling is a radio-frequency oscillating magnetic field, in our case produced by a pair of circular coils in series side by side above the atoms (see [5]).
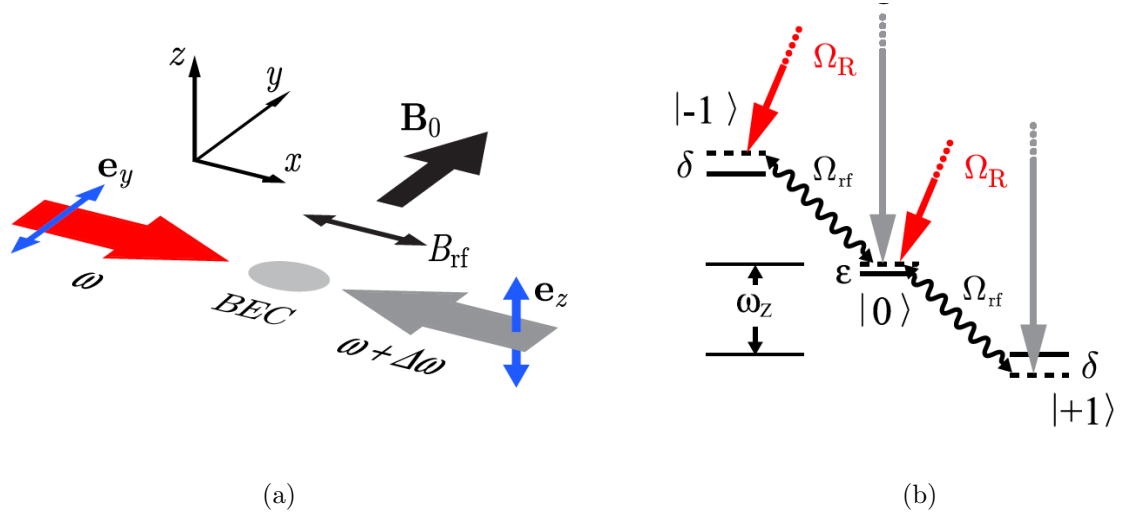
Hamiltonians

(a) (b)

Figure 5: Raman and rf coupling schematic. (a) Beam geometry of the Raman beams and rf relative to the external field. The Raman beams have a frequency difference $\Delta\omega$, and are linearly polarized in perpendicular directions. (b) Level structure of both Raman and Rf coupling for hyperfine states of the $F = 1$ manifold. The hyperfine splitting sparates the levels by an energy $\hbar\omega_z$. The quadratic Zeeman shift ϵ lowers the energy of the $m_F = 0$ state, and the detuning δ of either the Raman or the rf fields shifts the energies of the $m_F = \pm 1$ states. Raman transitions are two-photon, exciting up to a virtual state and coming back down to an adjacent hyperfine state, with an accompanying momentum transfer. Rf couples adjacent hyperfine states directly. Figure taken from ref. [6]

Figure: band structure bare/dressed rf/Raman

4.2.3 Calibration and adiabatic laoding of Raman and Rf dressed states

Figure: Pulsing experiments

Figure: Pictures of adiabatically loaded states

4.3 Synthetic dimensions

4.3.1 Lattice Hamiltonian with Raman coupling

4.3.2 Emergence of effective magnetic field

4.3.3 Eigenstates of the synthetic 2-D lattice

4.3.4 Observation of skipping orbits

Bibliography

[1] B. K. Stuhl, H.-I. Lu, L. M. Aycock, D. Genkina, and I. B. Spielman. Visualizing edge states with an atomic bose gas in the quantum hall regime. *Science*, 349(6255):1514–, Sep 2015.

[2] N.W. Ashcroft and N.D. Mermin. *Solid State Physics*. Saunders College, Philadelphia, 1976.

[3] Nicola Marzari, Arash A. Mostofi, Jonathan R. Yates, Ivo Souza, and David Vanderbilt. Maximally localized wannier functions: Theory and applications. *Rev. Mod. Phys.*, 84:1419–1475, Oct 2012.

[4] Daniel Adam Steck. Rubidium 87 d line data. Available online, http://steck.us/alkalidata, January 2015. revision 2.1.5.

[5] Karina Jimenez-Garcia. *Artificial Gauge Fields for Ultracold Neutral Atoms*. PhD thesis, Joint Quantum Institute, National Institute of Standards and Technology, and the University of Maryland, 2012.

[6] K. Jiménez-García, L. J. LeBlanc, R. A. Williams, M. C. Beeler, A. R. Perry, and I. B. Spielman. Peierls substitution in an engineered lattice potential. *Phys. Rev. Lett.*, 108:225303, May 2012.